



Article

# *ITGB6*-Knockout Suppresses Cholangiocarcinoma Cell Migration and Invasion with Declining *PODXL2* Expression

Yurie Soejima <sup>1,\*</sup>, Miho Takeuchi <sup>1</sup>, Nao Miyamoto <sup>1</sup>, Motoji Sawabe <sup>1</sup> and Toshio Fukusato <sup>2,†</sup>

<sup>1</sup> Department of Molecular Pathology, Graduate School of Medical and Dental Sciences, Tokyo Medical and Dental University, 1-5-45 Yushima, Bunkyo-ku, Tokyo 113-8510, Japan; apmi56230@gmail.com (M.T.); miyamt.mlab@tmd.ac.jp (N.M.); m.sawabe.mp@tmd.ac.jp (M.S.)

<sup>2</sup> General Medical Education and Research Center, Teikyo University, 2-11-1 Kaga, Itabashi-ku, Tokyo 178-8605, Japan; fukusato@med.teikyo-u.ac.jp

\* Correspondence: soejima.mp@tmd.ac.jp; Tel.: +81-3-5803-5375

† These authors contributed equally to this work.

**Abstract:** Intrahepatic cholangiocarcinoma (iCCA) is a heterogeneous bile duct cancer with a poor prognosis. Integrin  $\alpha\beta6$  ( $\beta6$ ) has been shown to be upregulated in iCCA and is associated with its subclassification and clinicopathological features. In the present study, two *ITGB6*-knockout HuCCT1 CCA cell lines (*ITGB6*-ko cells) were established using the clustered regulatory interspaced short palindromic repeats (CRISPR), an associated nuclease 9 (Cas9) system, and single-cell cloning. RNA sequencing analysis, real-time polymerase chain reaction (PCR), and immunofluorescent methods were applied to explore possible downstream factors. *ITGB6*-ko cells showed significantly decreased expression of integrin  $\beta6$  on flow cytometric analysis. Both cell lines exhibited significant inhibition of cell migration and invasion, decreased wound-healing capability, decreased colony formation ability, and cell cycle dysregulation. RNA sequencing and real-time PCR analysis revealed a remarkable decrease in podocalyxin-like protein 2 (*PODXL2*) expression in *ITGB6*-ko cells. Colocalization of *PODXL2* and integrin  $\beta6$  was also observed. S100 calcium-binding protein P and mucin 1, which are associated with CCA subclassification, were downregulated in *ITGB6*-ko cells. These results describe the successful generation of *ITGB6*-ko CCA cell clones with decreased migration and invasion and downregulation of *PODXL2*, suggesting the utility of integrin  $\beta6$  as a possible therapeutic target or diagnostic marker candidate.

**Keywords:** cholangiocarcinoma; integrin; *ITGB6*; CRISPR/Cas9; RNA-seq; *PODXL2*



**Citation:** Soejima, Y.; Takeuchi, M.; Miyamoto, N.; Sawabe, M.; Fukusato, T. *ITGB6*-Knockout Suppresses Cholangiocarcinoma Cell Migration and Invasion with Declining *PODXL2* Expression. *Int. J. Mol. Sci.* **2021**, *22*, 6303. <https://doi.org/10.3390/ijms22126303>

Academic Editor: Cristina Peña

Received: 14 April 2021

Accepted: 8 June 2021

Published: 11 June 2021

**Publisher's Note:** MDPI stays neutral with regard to jurisdictional claims in published maps and institutional affiliations.



**Copyright:** © 2021 by the authors. Licensee MDPI, Basel, Switzerland. This article is an open access article distributed under the terms and conditions of the Creative Commons Attribution (CC BY) license (<https://creativecommons.org/licenses/by/4.0/>).

## 1. Introduction

Cholangiocarcinoma (CCA) is a heterogeneous bile duct cancer with poor prognosis, usually classified as intrahepatic, perihilar, or distal, based on its anatomical location [1–4]. Intrahepatic CCA (iCCA) arises above the second-order bile ducts. iCCA accounts for 10–15% of primary liver cancers and is the second most common primary hepatic malignancy after hepatocellular carcinoma (HCC) [4]. iCCA is an aggressive malignancy with very poor outcomes. Although surgical resection is a potentially curative treatment for early-stage tumors, most patients have advanced disease at diagnosis. The incidence of iCCA has increased globally over the last few decades, whereas the incidences of perihilar CCA and distal CCA have decreased [1,4]. Therefore, iCCA warrants considerable attention.

iCCA can be further subclassified into two main subtypes: large duct type and small duct type [4]. Large duct iCCA arises in the large intrahepatic bile ducts near the hepatic hilus and resembles perihilar and extrahepatic distal CCA, exhibiting macroscopic periductal infiltrating patterns and intraductal growth. Small duct iCCA occurs primarily in the hepatic periphery and has a macroscopic mass-forming growth pattern. These

subtypes are evidenced in the immune and molecular features of the tumors and are related to patient prognosis [1–4].

Recent studies of iCCA suggest the presence of proliferative and inflammatory molecular subclasses that have different clinicopathological features and gene mutations [5], some of which may be candidates for targeted, personalized therapy. Further, there appear to be associations between the inflammation subclass and the large duct type and between the proliferation subclass and the small duct type [4]. However, the precise mechanisms of carcinogenesis and progression in iCCA are still unclear. In addition, because of the heterogeneity of iCCA and the emergence of chemoresistant clones, the development of more effective novel drugs and therapeutic strategies is warranted [6].

Studies from our laboratories have demonstrated that integrin  $\beta 6$  is highly expressed in iCCA, contrasting to its relatively low expression in cholangiolocellular carcinoma (CoCC) and HCC [7]. Integrins are heterodimeric cell surface receptors for cell adhesion and movement found in at least 24 unique combinations of alpha subunits (18 types) and beta subunits (8 types). They are regulated by inside-out signaling across the plasma membrane by cell-extracellular matrix and cell–cell adhesions [8,9]. Integrins are known to be important in cell migration and the regulation of cell proliferation and invasion in cancer [10,11]. Integrin  $\alpha v\beta 6$  ( $\beta 6$ ) is expressed exclusively on epithelial cells and is typically expressed only during tissue remodeling, embryogenesis, and carcinogenesis [12]. Integrin  $\beta 6$  is upregulated in several tumor types [13] and promotes invasion in several cancers, including colorectal cancer and pancreatic cancer, through the extracellular signal-regulated kinase and transforming growth factor (TGF)- $\beta$  pathways that promote matrix metalloproteinase activation [14–16]. It has been reported that integrin  $\beta 6$ -blocking antibody and antisense integrin  $\beta 6$  treatment suppress tumor growth in animal models, suggesting a possible role for integrin  $\beta 6$  blockade in cancer treatment [16]. In CCA, significant increases in expression of integrins  $\beta 6$  and  $\alpha 6$  and their usefulness as diagnostic and prognostic indicators have been reported [17–19].

Furthermore, in iCCA, integrin  $\beta 6$  is more highly expressed in the non-peripheral and periductal-infiltrating/intraductal growth types than in the peripheral and mass-forming types, reflecting a close association between integrin  $\beta 6$  expression and the subclassification of iCCA. This might occur mainly through the integrin  $\beta 6$  ligands, tenascin-C, and TGF- $\beta$  [20]. However, there is currently no direct or mechanistic evidence of the specific role of integrin  $\beta 6$  expression in modifying biological behaviors in iCCA.

The aim of this study was to generate *ITGB6*-knockout (*ITGB6*-ko) iCCA cell clones using clustered regulatory interspaced short palindromic repeats (CRISPR)/CRISPR-associated nuclease 9 (Cas9) gene editing and to confirm the specific effects of integrin  $\beta 6$  on the biological behaviors of iCCA cells. In addition, the molecules correlated with integrin  $\beta 6$  expression were investigated using RNA sequencing (RNA-seq) analysis and real-time polymerase chain reaction (PCR) analysis.

## 2. Results

### 2.1. Establishment of *ITGB6*-Knockout (ko) Cell Lines

After transfection and single-cell cloning, mutations in the cloned cells were confirmed by direct sequencing and comparison with HuCCT1 wild-type (HuCCT1-wt) cells. A clone with a heterozygous mutation was obtained after the first transfection. This clone was transfected again, which yielded two clones with two homozygous insertion–deletion mutations, *ITGB6*-ko 1 and -ko 2 (Table 1). Premature stop codons were detected in these clones. Integrin  $\beta 6$  protein was significantly reduced in these *ITGB6*-ko cell lines by both immunofluorescence staining (Figure 1A) and flow cytometry (Figure 1B). For flow cytometry, integrin  $\beta 6$  protein expression on the cell membrane and in the cytoplasm was evaluated and described as the mean fluorescence intensity multiplied by the percentage of integrin  $\beta 6$ -positive cells (Figure 1C). Integrin  $\beta 6$  expression was markedly reduced in *ITGB6*-ko cells such as HuH28 with a low-*ITGB6* mRNA level compared to HuCCT1-wt cells, indicating the successful establishment of *ITGB6*-ko cell lines.

**Table 1.** Direct sequence analysis of target genes in *ITGB6*-knockout monoclonal cells.

| HuCCT1             | Sequence of Target Genes                    | Results | Amino Acid  |
|--------------------|---|---------|-------------|
| wt                 | (T)CCATGGATGACGACCTCAAC                     |         | SMDDDLN     |
| <i>ITGB6</i> -ko 1 | (T)CCA <b>I</b> ITGGA <b>TGA</b> CGACCTCAAC | +1      | SIG(STOP)   |
| <i>ITGB6</i> -ko 2 | (T)CCA <b>I</b> ITGGA <b>TGA</b> CGACCTCAAC | +1      | SIG(STOP)   |
|                    | ATG-----ACCTCAACACAA <b>TAA</b> AGG         | -25     | MTSTQ(STOP) |

wt: wild-type, *ITGB6*-ko: integrin β6-knockout, stop codon: TAA; TAG; TGA.

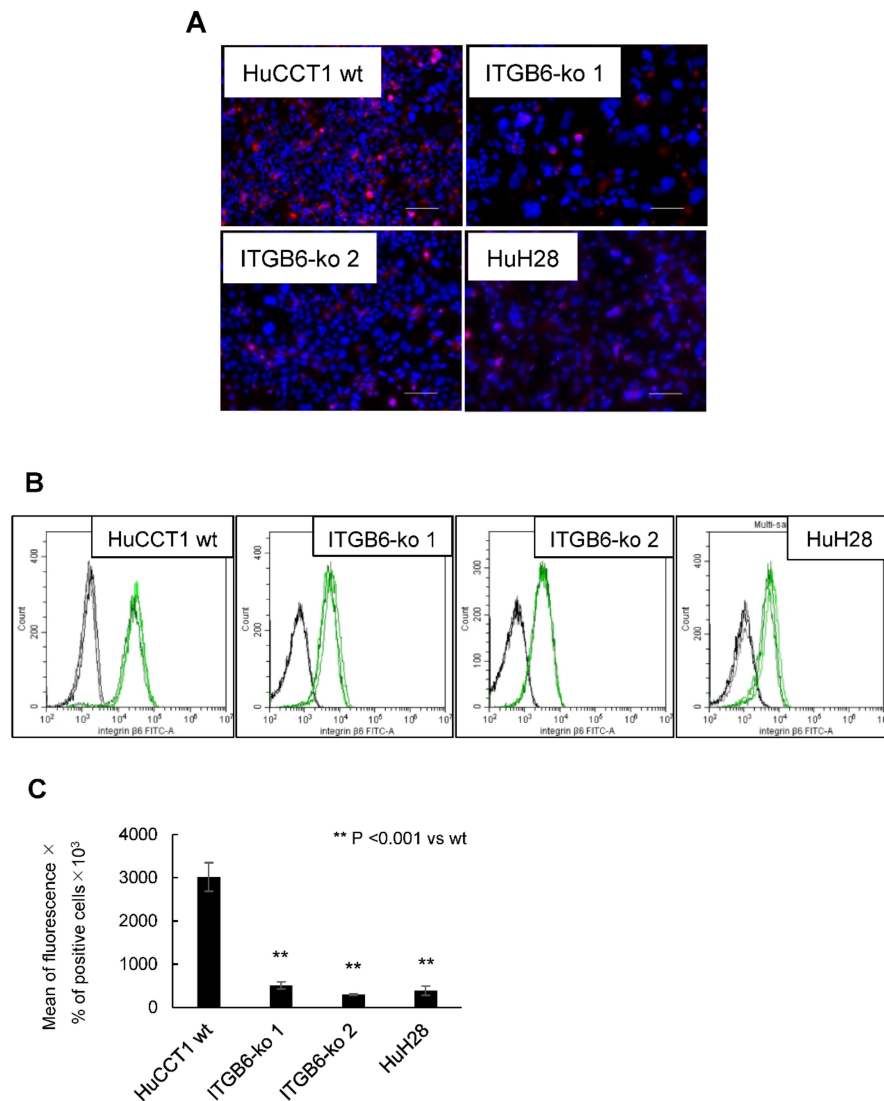


**Figure 1.** Integrin β6 protein was reduced in integrin β6-knockout (*ITGB6*-ko) cell lines by immunofluorescence staining and flow cytometry. (A) Integrin β6 staining (red) in the cytoplasm and plasma membrane of HuCCT1 wild-type (wt), *ITGB6*-ko cells, and HuH28 (scale bar, 100 μm). (B) Representative histograms for integrin β6 expression determined by flow cytometry (black lines, mouse IgG1; green lines, mouse monoclonal anti-integrin β6). (C) The mean fluorescence intensity was multiplied by the percentage of integrin β6-positive cells to determine integrin β6 expression. The expression of integrin β6 was significantly decreased in *ITGB6*-ko 1 and -ko 2 cells compared with HuCCT1-wt cells ( $p < 0.001$ ) as well as HuH28 cells as a negative control. Experiments were performed in triplicate.

## 2.2. *ITGB6*-Knockout Reduced the Migration and Invasion of iCCA Cells

The migration ability of *ITGB6*-ko 1 and -ko 2 cells was significantly reduced compared to that of HuCCT1-wt cells (migrated cells/field: wt,  $833.2 \pm 57.6$ ; *ITGB6*-ko 1,  $206.8 \pm 61.3$ ; and *ITGB6*-ko 2,  $160.4 \pm 11.2$ ;  $p < 0.001$ ) (Figure 2A,B). Similarly, the invasion ability of *ITGB6*-ko cells was also significantly reduced compared with that of HuCCT1-wt cells (invaded cells/field: wt,  $589.7 \pm 119.8$ ; *ITGB6*-ko 1,  $157.6 \pm 25.3$ ; and *ITGB6*-ko 2,  $144.7 \pm 12.7$ ;  $p < 0.001$ ) (Figure 2A,B). In the wound-healing assay, HuCCT1-wt cells migrated further in 96 h than *ITGB6*-ko 1 cells (remaining wound proportion:  $0.16 \pm 0.074$  versus  $0.37 \pm 0.053$ ,  $p < 0.001$ ). HuCCT1-wt cells also migrated further in 48 h than *ITGB6*-ko 2 cells (remaining wound proportion:  $0.48 \pm 0.11$  versus  $0.63 \pm 0.11$ ,  $p < 0.01$ ) (Figure 2C,D). These results indicated that the *ITGB6*-knockout significantly inhibited cell migration and invasion, as well as decreased wound-healing capability.

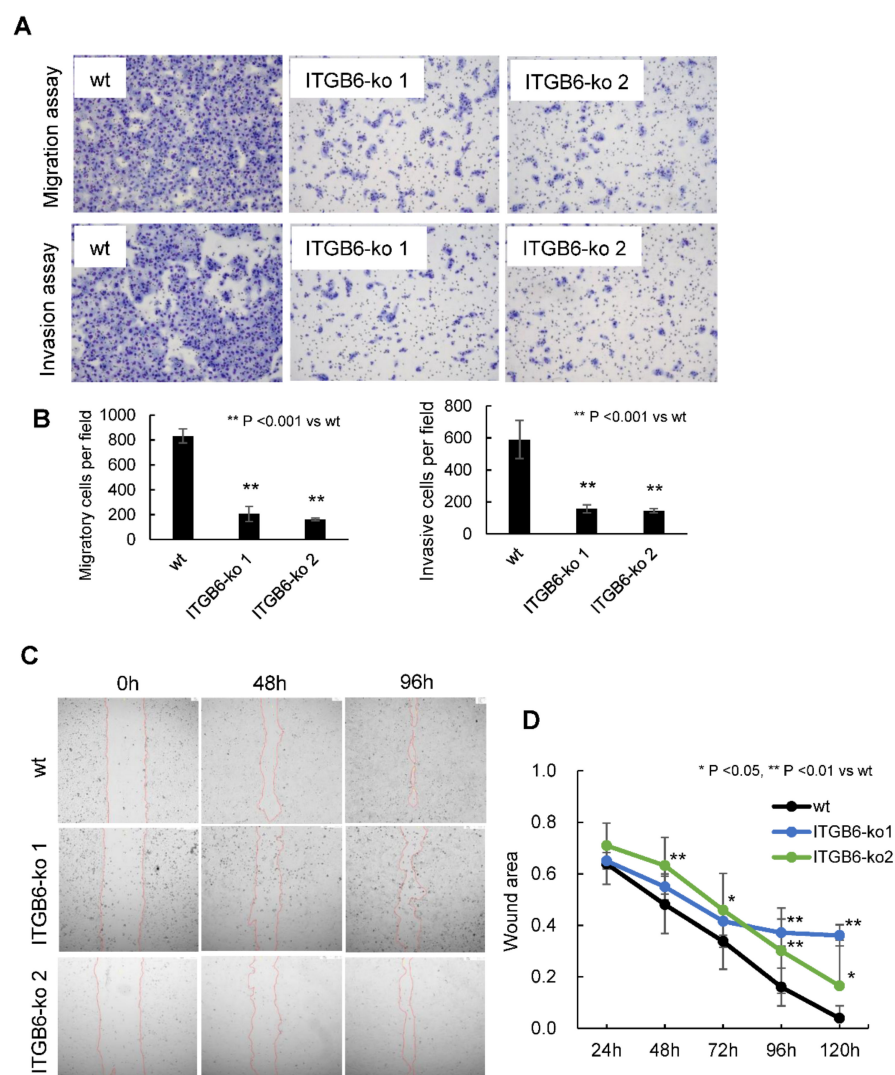


**Figure 2.** Integrin  $\beta 6$ -knockout (*ITGB6*-ko) cells have decreased patterns of migration and invasion. (A) Migratory and invasive cells were stained with Diff-Quik solution. (B) Migratory cells per field and invasive cells per field were significantly decreased in *ITGB6*-ko cells compared to wild-type (wt) cells ( $p < 0.001$  for both). The results shown represent the mean  $\pm$  standard deviation from three independent experiments. (C) Wound closure of HuCCT1-wt, *ITGB6*-ko 1, and *ITGB6*-ko 2 cells after scratching. (D) Quantitation of wound areas represent the results of three independent experiments. *ITGB6*-ko 1 and -ko 2 cells were significantly less migratory than wild-type cells.

### 2.3. *ITGB6*-Knockout Inhibited Colony Formation and Induced Cell Cycle Dysregulation in *iCCA* Cells

The colony formation abilities of *ITGB6*-ko 1 ( $78 \pm 20 \times 10^4 \mu\text{m}^2$ ) and *ITGB6*-ko 2 ( $45 \pm 8.6 \times 10^4 \mu\text{m}^2$ ) cells were significantly reduced to 48.9% and 28.3% compared to that of the HuCCT1-wt cells ( $160 \pm 46 \times 10^4 \mu\text{m}^2$ ) ( $p < 0.05$  and  $0.01$ , respectively) (Figure 3A,B), indicating decreased colony formation ability after *ITGB6*-knockout. We assessed cell cycle progression in *ITGB6*-ko cells by flow cytometry. The *ITGB6*-ko 1 and *ITGB6*-ko 2 cells had significantly fewer cells in the G0/G1 fractions than the HuCC1-wt cells (41% and 49%, respectively, versus 63%;  $p < 0.005$  for both), and they had significantly more cells in the S/G2/M fractions (43% and 37%, respectively, vs. 31%;  $p < 0.005$  and  $< 0.05$ , respectively) (Figure 3C,D). Therefore, *ITGB6*-knockout induced cell cycle dysregulation and increased the number of cells in the S/G2 phase. Furthermore, apoptotic responses evaluated by detection of activated caspase-3 were observed in *ITGB6*-ko 1 and *ITGB6*-ko2, while not in HuCCT1-wt (Figure 3E).

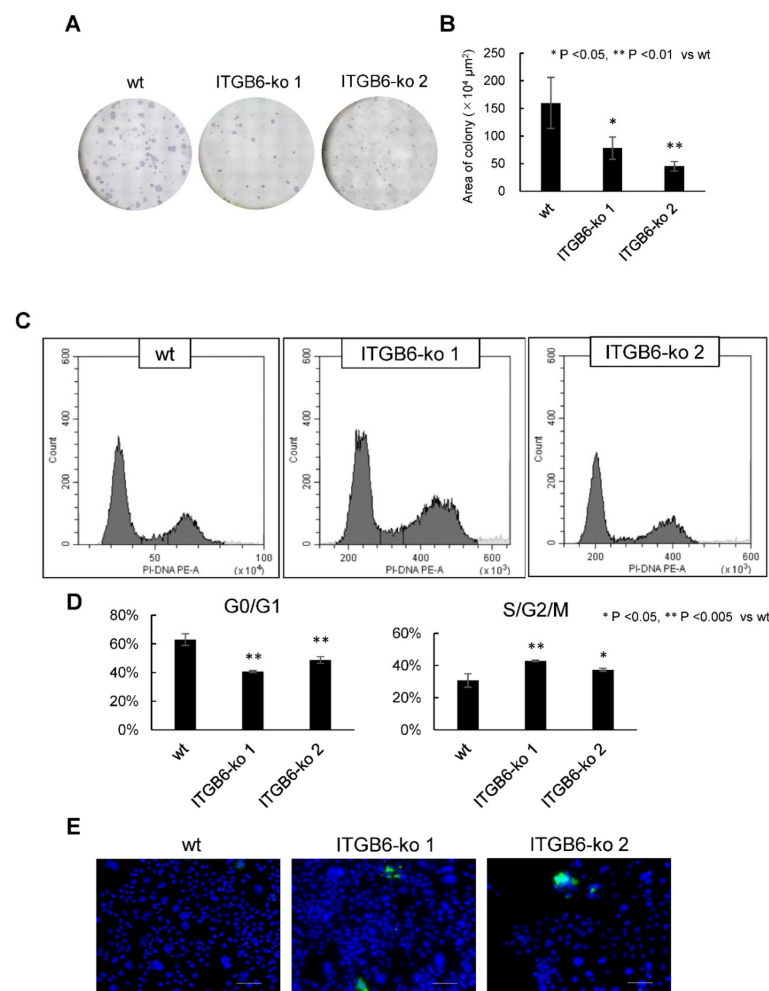


**Figure 3.** Integrin  $\beta 6$ -knockout (*ITGB6*-ko) affected colony formation and cell cycle progression. (A) Colonies were stained with crystal violet. (B) The *ITGB6*-ko cells colonies covered significantly less surface area than the wild-type (wt) cell colonies. (C) Representative histograms of cell distribution in each cell cycle phase determined by flow cytometry. (D) The number of cells in G0/G1 was lower in *ITGB6*-ko cells than in wt cells, whereas the number of cells in S/G2/M was increased in *ITGB6*-ko cells. All experiments were performed in triplicate. (E). Cleaved caspase-3 immunofluorescence was observed in *ITGB6*-ko cells, while not in wild-type cells. DAPI was used to stain nucleus. Green and blue signals indicate cleaved caspase-3 and nucleus respectively.

#### 2.4. RNA-Seq and Real-Time PCR Analysis Revealed a Significant Decrease in *PODXL2* Expression in *ITGB6*-ko Cells

RNA-seq analysis was applied to explore genes associated with *ITGB6*-knockout in iCCA cells. A total of 60,728 genes were expressed in *ITGB6*-ko and HuCCT1-wt cells. Gene ontology and pathway analysis were performed using genes with significantly different expression, i.e.,  $p < 0.05$  and  $\log_2$  fold change  $< -1$  ( $n = 479$ ) or  $\log_2$  fold change  $> 1$  ( $n = 621$ ). We focused on assessing the downregulated genes in *ITGB6*-ko 1 cells to explore genes with concordant expression with *ITGB* gene. In terms of biological process, we found decreased expression of genes involved in cell–cell signaling, extracellular matrix organization, and epithelial cell differentiation (Supplementary Table S1). A pathway analysis using the Kyoto Encyclopedia of Genes and Genomes (KEGG) database did not reveal significant pathways involved in migration, invasion, or proliferation (Supplementary Table S1). To identify genes closely related to *ITGB6*, we included only those genes with an adjusted  $p$ -value  $< 0.05$  and a  $\log_2$  fold change  $< -1$  ( $n = 38$ ) or a  $\log_2$  fold change  $> 1$  ( $n = 92$ ) and extracted genes with a large difference in expression between HuCCT1-wt and *ITGB6*-ko 1 cells (Supplementary Figure S1). The top 20 downregulated genes in *ITGB6*-ko 1 cells are shown in Table 2. The top 20 upregulated genes in *ITGB6*-ko cells are shown in Table 3.

In addition, to evaluate the possibility of interactive changes in integrin subunit genes, the expression of 35 integrin genes were comparatively examined in the RNA-seq data, but we observed no significant changes other than the slightly decreased expression of integrin subunit alpha E in *ITGB6*-ko 1 cells (data not shown).

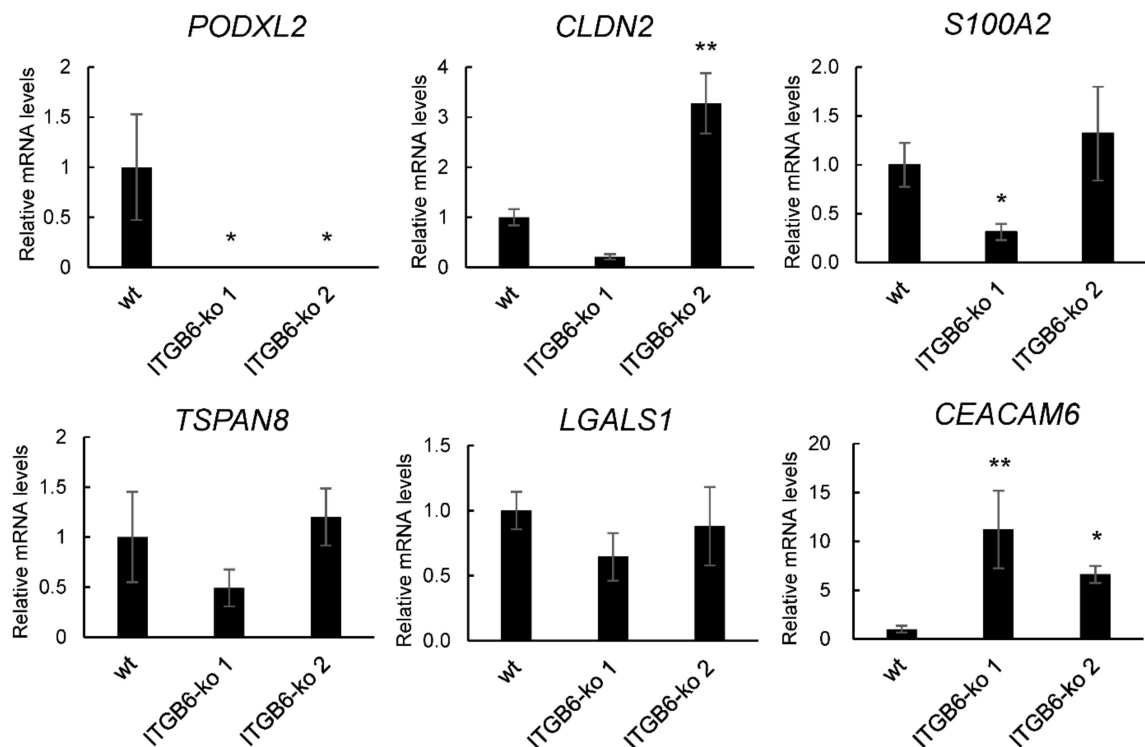
We were interested in downregulated genes in knockout cells for therapeutic strategy and selected 5 of the top 20 downregulated genes in *ITGB6*-ko 1 cells, podocalyxin-like 2 (*PODXL2*), claudin 2, S100 calcium-binding protein A2, tetraspanin 8, and galectin 1, which have been associated with cell migration and adhesion in previous studies, and one upregulated gene, CEA cell adhesion molecule 6 (*CEACAM6*), to validate the RNA-seq data using real-time PCR. *PODXL2* had the greatest (negative) fold change and was the most significantly downregulated gene concordantly in both *ITGB6*-ko 1 and *ITGB6*-ko 2 cells compared with HuCCT1-wt cells ( $p < 0.05$ ) (Figure 4), suggesting a possible relationship between *ITGB6* and *PODXL2* expression. *CEACAM6* expression was significantly increased concordantly in both *ITGB6*-ko 1 and *ITGB6*-ko 2 cells compared to HuCCT1-wt cells ( $p < 0.01$  and  $0.05$ , respectively) (Figure 4).

**Table 2.** Top 20 downregulated genes in *ITGB6*-knockout cholangiocarcinoma (HuCCT1) cell line.

| Entrez Gene ID | Gene Symbol | Gene Name                                    | Log2 Fold Change | Adjusted $p$ -Value |
|----------------|-------------|--|------------------|---------------------|
| 50512          | PODXL2      | podocalyxin-like 2                           | −7.50            | 0.021               |
| 5915           | RARB        | retinoic acid receptor beta                  | −4.42            | 0.015               |
| 93659          | CGB5        | chorionic gonadotropin subunit beta 5        | −2.91            | 0.017               |
| 23584          | VSIG2       | V-set and immunoglobulin domain-containing 2 | −2.88            | 0.023               |
| 9075           | CLDN2       | claudin 2                                    | −2.82            | 0.021               |
| 79966          | SCD5        | stearoyl-CoA desaturase 5                    | −2.59            | 0.045               |
| 4495           | MT1G        | metallothionein 1G                           | −2.42            | 0.045               |
| 6273           | S100A2      | S100 calcium-binding protein A2              | −2.23            | 0.025               |
| 9022           | CLIC3       | chloride intracellular channel 3             | −1.89            | 0.017               |
| 725            | C4BPB       | complement component 4-binding protein beta  | −1.83            | 0.045               |
| 56925          | LXN         | latexin                                      | −1.74            | 0.039               |
| 7103           | TSPAN8      | tetraspanin 8                                | −1.53            | 0.042               |
| 5054           | SERPINE1    | serpin family E member 1                     | −1.51            | 0.023               |
| 3956           | LGALS1      | galectin 1                                   | −1.35            | 0.017               |
| 8263           | F8A1        | coagulation factor VIII-associated 1         | −1.34            | 0.026               |
| 230            | ALDOC       | aldolase, fructose-bisphosphate C            | −1.21            | 0.019               |
| 1075           | CTSC        | cathepsin C                                  | −1.15            | 0.018               |
| 6319           | SCD         | stearoyl-CoA desaturase                      | −1.12            | 0.007               |
| 3149           | HMGB3       | high mobility group box 3                    | −1.08            | 0.021               |
| 39             | ACAT2       | acetyl-CoA acetyltransferase 2               | −1.03            | 0.017               |

**Table 3.** Top 20 upregulated genes in *ITGB6*-knockout cholangiocarcinoma (HuCCCT1) cell line.

| Entrez Gene ID | Gene Symbol | Gene Name   | Log2 Fold Change | Adjusted <i>p</i> -Value |
|----------------|-------------|---|------------------|--------------------------|
| 3620           | IDO1        | indoleamine 2,3-dioxygenase 1                               | 4.88             | 0.036                    |
| 2537           | IFI6        | interferon alpha inducible protein 6                        | 3.41             | 0.044                    |
| 4680           | CEACAM6     | CEA cell adhesion molecule 6                                | 3.05             | 0.028                    |
| 91543          | RSAD2       | radical S-adenosyl methionine domain-containing 2           | 2.91             | 0.017                    |
| 27074          | LAMP3       | lysosomal associated membrane protein 3                     | 2.90             | 0.015                    |
| 4600           | MX2         | MX dynamin-like GTPase 2                                    | 2.84             | 0.017                    |
| 4599           | MX1         | MX dynamin-like GTPase 1                                    | 2.79             | 0.030                    |
| 4939           | OAS2        | 2'-5'-oligoadenylate synthetase 2                           | 2.67             | 0.017                    |
| 8638           | OASL        | 2'-5'-oligoadenylate synthetase-like                        | 2.67             | 0.014                    |
| 8519           | IFITM1      | interferon-induced transmembrane protein 1                  | 2.62             | 0.040                    |
| 9636           | ISG15       | ISG15 ubiquitin-like modifier                               | 2.61             | 0.008                    |
| 115361         | GBP4        | guanylate-binding protein 4                                 | 2.57             | 0.047                    |
| 3437           | IFIT3       | interferon-induced protein with tetratricopeptide repeats 3 | 2.55             | 0.017                    |
| 81030          | ZBP1        | Z-DNA-binding protein 1                                     | 2.48             | 0.011                    |
| 4938           | OAS1        | 2'-5'-oligoadenylate synthetase 1                           | 2.43             | 0.008                    |
| 10406          | WFDC2       | WAP four-disulfide core domain 2                            | 2.38             | 0.031                    |
| 3075           | CFH         | complement factor H   | 2.38             | 0.022                    |
| 3434           | IFIT1       | interferon-induced protein with tetratricopeptide repeats 1 | 2.36             | 0.017                    |
| 25984          | KRT23       | keratin 23  | 2.31             | 0.008                    |
| 3433           | IFIT2       | interferon-induced protein with tetratricopeptide repeats 2 | 2.30             | 0.018                    |

\**P* < 0.05, \*\**P* < 0.01

**Figure 4.** Real-time polymerase chain reaction analysis. mRNA levels of podocalyxin-like 2 (*PODXL2*) were significantly decreased concordantly in both integrin  $\beta 6$ -knockout (ko) 1 and -ko 2 cells compared with HuCCCT1 wild-type cells, whereas CEA cell adhesion molecule 6 (*CEACAM6*) mRNA levels were increased concordantly. The mRNA level of claudin 2 was significantly increased in *ITGB6*-ko 2 cells, and S100 calcium-binding protein A2 mRNA level was significantly decreased in *ITGB6*-ko 1 while tetraspanin 8 and galectin 1 showed no significant change. All experiments were performed in triplicate.

### 2.5. Immunofluorescence Staining of PODXL2, CEACAM6, S100P, MUC1, and CD56

Immunofluorescence staining was performed to investigate the protein expression of PODXL2 and CEACAM6 in HuCCT1-wt and *ITGB6*-ko cells. PODXL2 was expressed in the cytoplasm and plasma membrane of HuCCT1-wt cells, and its expression was decreased in *ITGB6*-ko cells (Figure 5A). In addition, it was evident from double immunofluorescence staining that PODXL2 was colocalized with integrin  $\beta 6$  in HuCCT1-wt cells (Figure 5A). CEACAM6 was localized to the cell membrane and cytoplasm, and its expression was higher in *ITGB6*-ko cells than in HuCCT1-wt cells (Figure 5B).

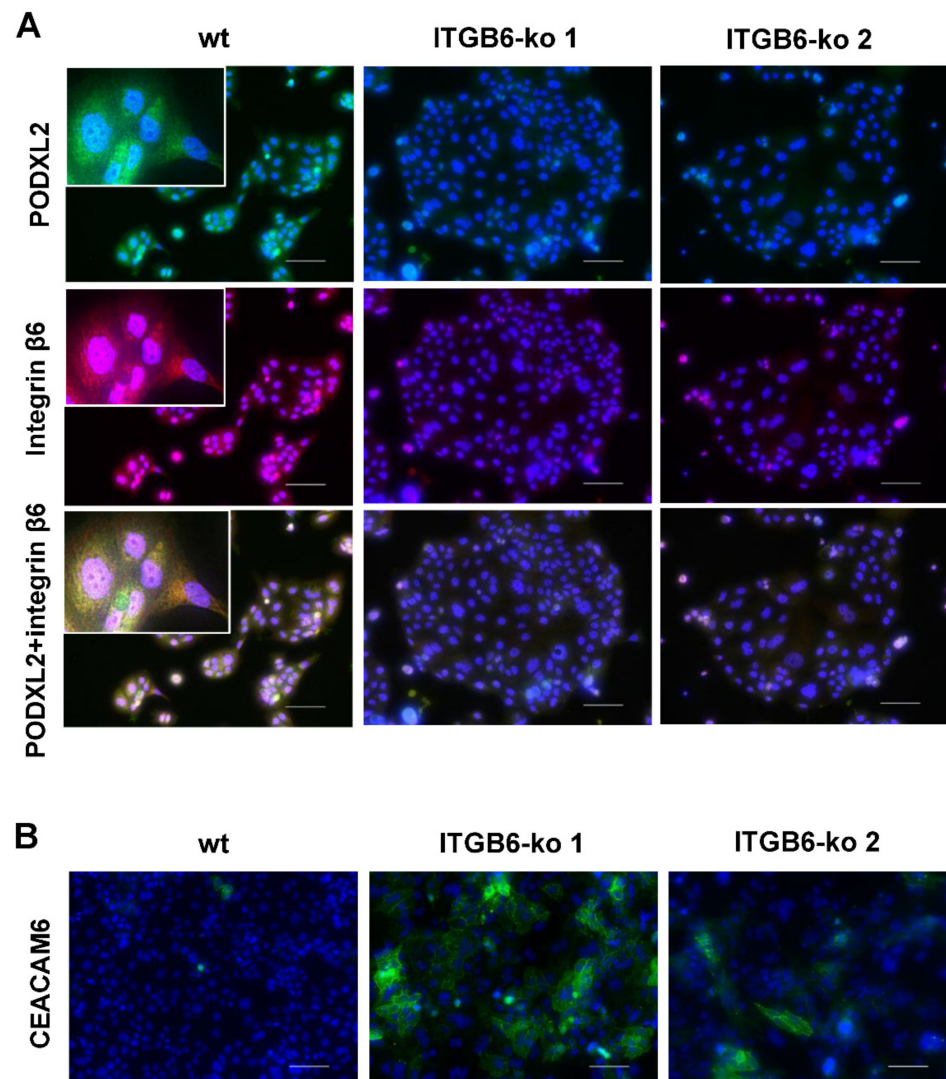


**Figure 5.** Immunofluorescence staining of podocalyxin-like protein 2 (PODXL2), integrin  $\beta 6$ , and CEA cell adhesion molecule 6 (CEACAM6) in HuCCT1 wild-type (wt) and integrin  $\beta 6$ -knockout (*ITGB6*-ko) cells. (A) PODXL2 (green) was strongly expressed in HuCCT1-wt cells and significantly downregulated in *ITGB6*-ko cells. The expression of integrin  $\beta 6$  is shown in red. Merged images of PODXL2 and integrin  $\beta 6$  are yellow (inset), indicating colocalization of PODXL2 and integrin  $\beta 6$ . (B) CEACAM6 was localized to the cell membrane and cytoplasm and was increased in *ITGB6*-ko cells compared with wild-type cells. (Scale bar, 100  $\mu\text{m}$ ).

S100 calcium-binding protein P (S100P) and mucin 1 (MUC1), which are markers for large bile duct iCCA, were decreased in *ITGB6*-ko 1 and -ko 2 cells compared to HuCCT1-wt cells, whereas CD56 (also called neural cell adhesion molecule), a marker for small bile duct iCCA, was slightly increased in *ITGB6*-ko 1 (Figure 6). These results suggested that proteins that are predominant in large bile duct iCCA are downregulated in *ITGB6*-ko cells.

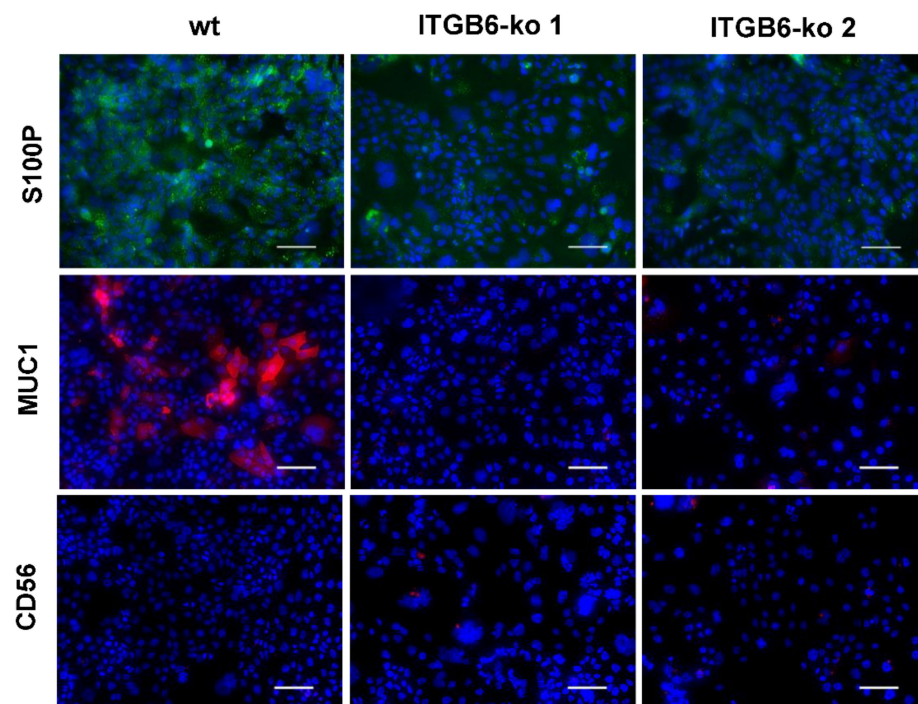


**Figure 6.** Immunofluorescence staining of S100 calcium-binding protein P (S100P), mucin 1 (MUC1), and CD56 in HuCCT1 wild-type (wt) and integrin  $\beta$ 6-knockout (*ITGB6*-ko) cells. The expressions of S100P (green) and MUC1 (red) decreased in *ITGB6*-ko cells compared with wild-type cells, whereas the expression of CD56 (red) showed slight increase in *ITGB6*-ko 1. (Scale bar, 100  $\mu$ m).

#### 2.6. Relationship between PODXL2 Expression and Clinicopathological Features in Patients with Intrahepatic Cholangiocarcinoma (iCCA)

Positive immunohistochemical staining for PODXL2 were observed in 17 (32.7%) of 52 iCCAs. PODXL2 expression was localized in the cell membrane and cytoplasm. The correlations between PODXL2 expression and the localization, histological differentiation, growth type, serosa invasion, and bile duct invasion of iCCA were statistically significant (Table 4). PODXL2 expression was higher in the non-peripheral central localization type iCCA than in the peripheral localization type ( $p = 0.0197$ ); lower in the poorly differentiated type than in the well-differentiated type ( $p = 0.0104$ ); and higher in the infiltrative-growth type than in the expansive-growth type ( $p = 0.0223$ ). High expression was related to serosa invasion and bile duct invasion ( $p = 0.0239$  and  $0.0038$ , respectively).

**Table 4.** Relationship between PODXL2 expression and clinicopathological characteristics of intrahepatic cholangiocarcinoma.

|                              |                      | Number of Cases<br>( $n = 52$ ) | PODXL2 Expression     |                       | $p$ -Value |
|------------------------------|----------------------|---------------------------------|-----------------------|-----------------------|------------|
|                              |                      |                                 | Negative ( $n = 35$ ) | Positive ( $n = 17$ ) |            |
| Gender                       | Male                 | 39                              | 26                    | 13                    | 0.575      |
|                              | Female               | 13                              | 9                     | 4                     |            |
| Age (mean) (years)           |                      |                                 | 73.9 (39–84)          | 73.7 (51–81)          | 0.731      |
| Tumor size (mean) (mm)       |                      |                                 | 66.2 (18–220)         | 63.9 (20–114)         | 0.519      |
| Localization                 | Peripheral           | 41                              | 31                    | 10                    | 0.0197 *   |
|                              | Non-peripheral       | 11                              | 4                     | 7                     |            |
| Macroscopic type             | MF                   | 46                              | 33                    | 13                    | 0.0808     |
|                              | MF + PI, IG + PI, PI | 6                               | 2                     | 4                     |            |
| Histological differentiation | Well                 | 7                               | 3                     | 4                     | 0.0104 *   |
|                              | Moderate             | 32                              | 19                    | 13                    |            |

Table 4. Cont.

|                         |              | Number of Cases<br>(n = 52) | PODXL2 Expression |                   | p-Value   |
|-------------------------|--------------|-----------------------------|-------------------|-------------------|-----------|
|                         |              |                             | Negative (n = 35) | Positive (n = 17) |           |
| Growth type             | Poor         | 13                          | 13                | 0                 | 0.0223 *  |
|                         | Expansive    | 24                          | 20                | 4                 |           |
|                         | Infiltrative | 28                          | 15                | 13                |           |
| Serosa invasion         | +            | 25                          | 13                | 12                | 0.0239 *  |
|                         | −            | 27                          | 22                | 5                 |           |
| Portal vein invasion    | +            | 42                          | 27                | 15                | 0.290     |
|                         | −            | 10                          | 8                 | 2                 |           |
| Hepatic vein invasion   | +            | 22                          | 13                | 9                 | 0.217     |
|                         | −            | 30                          | 22                | 8                 |           |
| Hepatic artery invasion | +            | 5                           | 3                 | 2                 | 0.533     |
|                         | −            | 47                          | 32                | 15                |           |
| Bile duct invasion      | +            | 27                          | 13                | 13                | 0.0038 ** |
|                         | −            | 25                          | 22                | 3                 |           |
| Intrahepatic metastasis | +            | 21                          | 12                | 9                 | 0.162     |
|                         | −            | 31                          | 23                | 8                 |           |
| Lymph node metastasis   | +            | 14                          | 8                 | 6                 | 0.266     |
|                         | −            | 38                          | 27                | 11                |           |

MF: mass-forming type, PI: periductal-infiltrating type, IG: intraductal-growth type; \*,  $p < 0.05$ ; \*\*,  $p < 0.01$ .

### 2.7. Correlation between Integrin $\beta 6$ Expression and PODXL2 Expression in iCCA Tissues

The expression of integrin  $\beta 6$  was observed in 31 (59.6%) of iCCA. In this study, integrin  $\beta 6$  expression was considered positive when more than 5% of the tumor cells or areas showed positive staining. The localization of integrin  $\beta 6$  expression was in cell membrane, cytoplasm, and basal lamina. Integrin  $\beta 6$  expression was associated with macroscopic type ( $p = 0.0362$ ), intrahepatic metastasis ( $p = 0.0417$ ), and lymph node metastasis ( $p = 0.0194$ ) (Supplementary Table S2). Furthermore, PODXL2 expression was significantly correlated with integrin  $\beta 6$  expression within tumors ( $r = 0.569$ ,  $p = 0.000049$ ) (Figure 7).

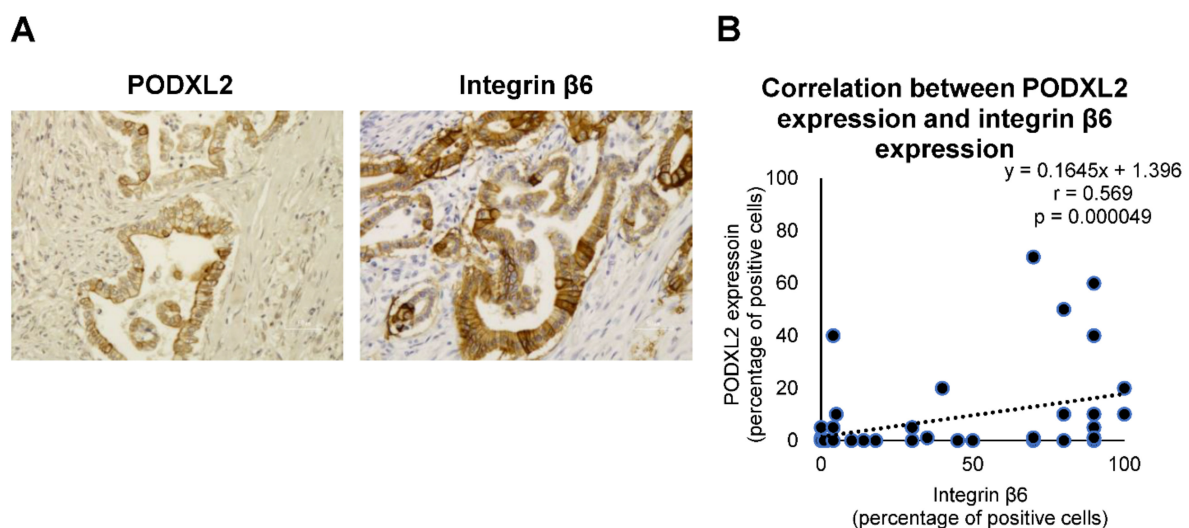


**Figure 7.** Expressions of PODXL2 and integrin  $\beta 6$  in intrahepatic cholangiocarcinoma tissue. (A) PODXL2 and integrin  $\beta 6$  are shown in the cell membrane and cytoplasm of tumor cells. PODXL2 expression patterns resemble integrin  $\beta 6$  expression patterns. Scale bar, 50  $\mu\text{m}$ . (B) Correlation between PODXL2 expression and integrin  $\beta 6$  expression within tumors was significant ( $r = 0.569$ ,  $p = 0.000049$ ).

### 3. Discussion

In this study, *ITGB6*-ko iCCA cell lines were generated using the CRISPR/Cas9 system and single-cell cloning. Direct sequence analysis after transfection of gRNAs into HuCCT1 cells showed a single-base insertion in the HuCCT1 *ITGB6*-ko 1 line and a single-base insertion and large deletion in the HuCCT1 *ITGB6*-ko 2 line. Since these two clones do not have the original sequence of *ITGB6*, we regarded them as *ITGB6*-ko cell lines with homozygous mutations and a premature stop codon, although the effects of a large deletion in *ITGB6*-ko 2 line was not evaluated sufficiently. To confirm this, we performed immunofluorescence staining and flow cytometry, which indicated significantly decreased expression of integrin  $\beta 6$  protein in these cell lines compared with the HuCCT1-wt cells. Integrin  $\beta 6$  is the rate-limiting subunit for  $\alpha v\beta 6$  heterodimer formation. The expression of integrin  $\alpha v\beta 6$  is limited by the transcription of *ITGB6*, which is regulated by promoter-binding sites and phosphorylation of transcriptional factors, including signal transducer and activator of transcription (STAT) 3, CCAAT enhancer-binding protein alpha (C/EBP $\alpha$ ), ETS proto-oncogene 1 transcription factor (ETS1), and SMAD family member 3 (SMAD3). In our preliminary study using iCCA cell lines with significantly high and low integrin  $\beta 6$  expression (HuCCT1 and HuH28, respectively), no significant mutations in *ITGB6* or its promoter, except for a few silent mutations, were detected by direct sequencing analysis (unpublished data), suggesting that integrin  $\beta 6$  expression is not regulated by *ITGB6* gene mutation but by transcription.

After establishing these *ITGB6*-ko cell lines, the effects of the *ITGB6*-knockout on the biological behaviors and functions of iCCA cells were evaluated. Cell migration and invasion were markedly decreased in *ITGB6*-ko cells (*ITGB6*-ko 1 and -ko 2) in transwell assays and wound-healing assays when compared with HuCCT1-wt cells. Colony formation ability was also reduced in both knockout cell lines. In a previous study using integrin  $\beta 6$ -specific siRNA in CCA cells (RBE and QBC939), cell migration, invasion, and proliferation were significantly suppressed by integrin  $\beta 6$  silencing [18]. *ITGB6*-knockout in this study also inhibited cell migration and invasion, decreased colony formation, and affected cell cycle progression and apoptosis, indicating the close involvement of integrin  $\alpha v\beta 6$  in the regulation of migration, invasion, and proliferation in iCCA, as has been previously observed in other cancers [15,16].

We previously reported that integrin  $\beta 6$  was significantly downregulated in CoCC of low-grade malignant potential but upregulated in iCCA of aggressive malignant potential [7]. In addition, our previous study revealed the increased expression of integrin  $\beta 6$  in the central large bile duct and periductal infiltrating subtypes of iCCA, indicating a close relationship with iCCA subclassification [20]. In the present study, S100P and MUC1, proteins that are highly expressed in large bile duct iCCA [21,22], were decreased in the *ITGB6*-ko cell lines. These results suggest that HuCCT1 cells may have the characteristics of large bile duct iCCA but transform into small bile duct iCCA-like cells after integrin  $\beta 6$  suppression. The phenotypic change between large duct type and small duct type is interesting because previous studies have shown that small duct iCCA has a higher 5-year postoperative survival rate than large duct iCCA [4,21]. As the iCCA subtypes are based on mucin productivity and immunophenotype [4,22], our results suggest that integrin  $\beta 6$  might be a useful target for therapeutic and diagnostic strategies.

After we observed that *ITGB6*-knockout induced profound effects on iCCA cells and modified their biological behaviors, we wanted to determine the precise molecular pathways affected by integrin  $\beta 6$  and its specific effects in these cell lines. Therefore, we investigated the differentially regulated genes in *ITGB6*-ko cells using RNA-seq and real-time PCR analysis. The results showed a remarkable decline in *PODXL2* expression in both *ITGB6*-ko cell lines compared to the wild-type HuCCT1 cells. *PODXL2* is a newly discovered member of the CD34 family and a type-I transmembrane sialomucin that functions as an L-selectin ligand [23–25]. The role of *PODXL2* in cancer is not yet known, and no interacting partners or regulators have been identified. However, *PODXL1*, another CD34 family member, is overexpressed in several cancers, and high *PODXL1* is closely

associated with a poor prognosis in cancer patients [26,27]. In the present study, we demonstrated a possible relationship between PODXL2 and integrin  $\beta 6$ . A significant decrease in PODXL2 expression might be associated with decreased migration and invasion, as well as decreased colony formation, in *ITGB6*-ko iCCA cells. In BT474 breast cancer cells, knockdown of PODXL2 slightly suppressed tumor cell migration and reduced expression of cancer stem cell markers through the Rac family small GTPase 1 pathway [28]. Inhibition of colony formation in *ITGB6*-ko iCCA cells in the present study might also be induced by reduced expression of PODXL2, because PODXL2 might be necessary for the maintenance of clonogenic potential in CCA cells as indicated in breast cancer cells. In addition, it is interesting that PODXL2 was colocalized with integrin  $\beta 6$  in HuCCT1 cells, suggesting a close association between these two adhesion molecules. Furthermore, the relationship between PODXL2 expression and clinicopathological features in iCCA patients and significant correlation between integrin  $\beta 6$  expression and PODXL2 expression in iCCA tissues was also evident in the present immunohistochemical studies.

CRISPR/Cas9 is widely used as a gene-editing method to investigate the molecular basis of cancers [29,30]. The gRNA sequence has a crucial role in the efficiency and specificity of CRISPR/Cas9 by reducing off-target effects [31]. In the present study, we used this novel, powerful gene-editing tool to explore new molecules in the integrin pathway within iCCA cells and observed a close association between integrin  $\beta 6$  and PODXL2, which was first described in the present study. However, the precise role of PODXL2 in the integrin pathway is still unknown, so further studies evaluating the transcriptional regulation of both *ITGB6* and *PODXL2* through phosphorylation of transcription factors such as STAT3, C/EBP $\alpha$ , and SMAD3 in *ITGB6*-ko iCCA cells are warranted. In addition, the effect of integrin  $\beta 6$  on the invasive growth of iCCA cells in vivo has not yet been evaluated. In future studies, we want to establish a xenograft tumor model in nude mice bearing *ITGB6*-ko iCCA cells.

The present study is the first to successfully generate *ITGB6*-ko iCCA cell clones, which had decreased migration and invasion in vitro, as well as downregulation of PODXL2, suggesting the utility of integrin  $\beta 6$  as a possible therapeutic or diagnostic candidate. Because of its epithelium-specificity and its dependency on specific pathological conditions, integrin  $\beta 6$  expression has high affinity and de novo expression in cancer tissues and represents a promising cancer cell target [14]. We were interested in downregulated genes in knockout cells for therapeutic strategy. Application of integrin  $\beta 6$ -specific function blocking monoclonal antibodies and nonpeptidic and peptidic integrin ligands with antagonizing effects has been considered as a potential therapeutic approach [14,16,32]. Furthermore, imaging for cancers using novel integrin  $\beta 6$  ligands encourages a promising tool for cancer diagnosis [14,33].

## 4. Materials and Methods

### 4.1. Cell Line and Cell Culture

The human CCA cell line, HuCCT1 [34] and HuH28 [35] (Health Science Research Resources Bank, Osaka, Japan), which have significantly high and low expression of *ITGB6* mRNA, respectively [7], was maintained in RPMI-1640 medium (Sigma–Aldrich, St. Louis, MO, USA) supplemented with 10% fetal bovine serum (FBS) (Sigma–Aldrich) and 1% antibiotic-antimycotic (Gibco, Dublin, Ireland) in a humidified atmosphere at 37 °C with 5% CO<sub>2</sub>. These two cell lines were selected after previous experiments using five CCA cell lines with different characteristics reflecting heterogeneous cancer [7].

### 4.2. Patients and Tissue Samples

Tissue samples from 52 patients with iCCA were obtained by surgical resection at Tokyo Medical and Dental University Hospital between 2007–2018. Tissue samples were fixed in a 10% formalin solution, and embedded in paraffin for histological diagnosis and immunohistochemistry analysis. The patients included 39 men and 13 women ranging from 39 to 84 years of age (mean, 70.8 years). Six patients were positive for the serum hepatitis

B surface antigen (HBsAg), and eight were positive for the anti-hepatitis C virus (HCV) antibody; one was positive for both, and 39 were negative for both. The largest tumor diameters ranged from 18 to 220 mm (mean, 58.9 mm). iCCA was grossly classified into three groups: mass-forming (MF), periductal-infiltrating (PI), and intraductal-growth (IG), as well as mixed types (MF + PI and IG + PI). Based on surgical findings and macroscopic examination, the tumors were defined as peripheral localization types involving the septal and interlobular bile ducts, or as non-peripheral central localization types involving the first branches of the right and left hepatic bile ducts. The histological differentiation grades for iCCA were assigned according to World Health Organization classifications [4]. The surrounding non-tumorous liver tissues showed normal liver in 33 patients, chronic hepatitis in 12 patients, and cirrhotic change in seven patients. The diagnosis of iCCA was confirmed by immunohistochemical results that were positive for cytokeratin 7 and negative for hepatocyte marker (Hep Par-1), in addition to the histological findings. This study was approved by the ethics committee of Tokyo Medical and Dental University (No. M2000-2081; 8 May 2015).

#### 4.3. Transfection and Genomic Cleavage Detection

HuCCT1 cells ( $5 \times 10^4$  cells) with high expression of *ITGB6* mRNA were cultured in 24-well plates to subconfluency, transfected with guideRNA (gRNA; #1, #2, or #3), and True-Cut Cas9 Protein v2 (Invitrogen, Carlsbad, CA, USA) using Lipofectamine CRISPRMAX Cas9 Transfection Reagent (Invitrogen) in accordance with the manufacturer's protocols, and cultured for 48 h. gRNAs (TrueGuide Synthetic gRNAs, Invitrogen) against *ITGB6* were designed to be complementary to three target DNA sequences (#1, #2, and #3) (Figure 8). Genomic DNA cleavage efficiency was analyzed using the Gene Art Genomic Cleavage Detection Kit (Invitrogen). Briefly, primers for PCR amplification were designed (Supplementary Table S3), and DNA extraction and PCR amplification of target sequences were followed by enzyme treatment, in accordance with the manufacturer's protocol. After agarose gel electrophoresis, each band pattern was evaluated using image analysis software (ImageJ, National Institute of Health, Bethesda, MD, USA) to calculate the cleavage efficiency. Finally, transfection for gene knockout was performed in a 6-well plate ( $2.5 \times 10^5$  cells) using the gRNA #2 with the highest cleavage efficiency. gRNA #1 and #3 with low cleavage efficiency were not used in the following transfection experiment for gene knockout.

#### *ITGB6*

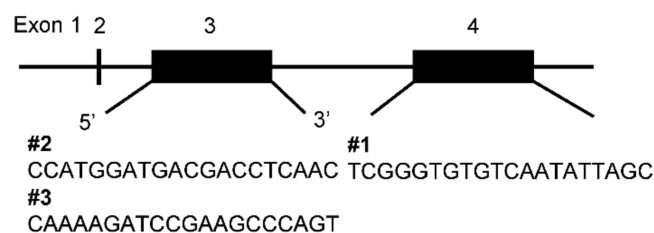


**Figure 8.** guideRNAs were designed complementary to target DNA sequences (#1–3) in exon 3 and exon 4 of integrin  $\beta 6$  (*ITGB6*).

#### 4.4. Single-Cell Cloning and Direct Sequence Analysis

After transfection, HuCCT1 cells were seeded into a 96-well plate at a concentration of 0.5 cells/well. Single cells were identified under the microscope and subcultured into 24-well plates after single-cell outgrowth. DNA was extracted from each monoclonal line using a QIAamp DNA Mini Kit (Qiagen, Hilden, Germany). After PCR, the amplicons of the target sequences were directly sequenced (FASMAC, Atsugi, Japan) to determine mutations. Sequencing was performed after TA cloning (TOPO TA Cloning Kit; Invitrogen) for some samples.

#### 4.5. Immunofluorescence Staining

Immunofluorescence staining was used to verify whether integrin  $\beta 6$  protein was reduced in the *ITGB6*-ko HuCCT1 clones and to investigate the expression of S100P, MUC1, CD56, PODXL2, CEACAM6, and cleaved caspase-3 in these clones. HuCCT1-wt cells, cells transfected with *ITGB6* gRNAs (*ITGB6*-ko) and HuH28 ( $5 \times 10^4$  cells) were cultured in 4-well chamber slides (IWAKI, Tokyo, Japan) to subconfluency and fixed in 4% paraformaldehyde/phosphate-buffered saline (PFA/PBS), followed by permeabilization with 0.1% Triton X-100/PBS for 10 min. After treatment with C-Block (casein-blocking solution; Genemed Biotechnologies, South San Francisco, CA, USA) for 20 min at room temperature, cells were incubated with mouse anti-integrin  $\beta 6$  (1:100; Merck, Darmstadt, Germany), rabbit anti-S100P (1:200; Abcam, Cambridge, UK), mouse anti-MUC1 (1:100; Novocastra Laboratories, Newcastle upon Tyne, UK), mouse anti-CD56 (1:100; Novocastra), rabbit anti-PODXL2 (1:200; Atlas Antibodies, Bromma, Sweden), rabbit anti-CEACAM6 (1:500; Abcam), or rabbit anti-cleaved caspase-3 (Asp175) (1:400; Cell signaling Technology, Danvers, MA, USA) antibodies overnight at 4 °C. After washing with 0.1% Tween 20/PBS, the cells were incubated with fluorescence-labeled secondary antibodies (goat anti-mouse IgG H&L, Alexa Fluor 594) goat anti-rabbit IgG H&L, Alexa Fluor 488; Abcam, diluted 1:1000) for 1 h at room temperature. Nuclei were stained with DAPI (Invitrogen). Stained cells were mounted with a fluorescence mounting medium (DAKO, Glostrup, Denmark) and examined using a Keyence BZ-X700 microscope (Keyence, Osaka, Japan). Double immunofluorescence staining for integrin  $\beta 6$  and PODXL2 was also performed, and the merged images were observed to assess colocalization.

#### 4.6. Flow Cytometry

We also confirmed the expression of integrin  $\beta 6$  in HuCCT1-wt and *ITGB6*-ko cells by flow cytometry as well as HuH28 cells as a control. Both membranous and intracellular integrin  $\beta 6$  were examined. Cells ( $1 \times 10^5$ – $10^6$ ) were collected and fixed with 4% PFA/PBS at room temperature for 15 min. After washing with 1% FBS/PBS, cell membranes were permeabilized with 0.1% Triton-X/PBS at room temperature for 10 min. Cells were incubated with mouse monoclonal anti-integrin  $\beta 6$  (1:100; Merck) as the primary antibody and mouse IgG1 (1:100; DAKO) as an isotype control for 30 min at 4 °C. After washing with 1% FBS/PBS, cells were incubated with fluorescently labeled goat anti-mouse IgG H&L antibody (Alexa Fluor 488, Abcam, 1:2000) for 30 min at 4 °C, and then the stained cells were analyzed by flow cytometry (CytoFLEX, BECKMAN COULTER, Brea, CA, USA).

#### 4.7. In Vitro Transwell Migration and Invasion Assays

Five hundred microliters of serum-free RPMI-1640 medium were placed into Matrigel-coated inserts and wells of the invasion chambers (Corning, NY, USA), which were placed at 37 °C for 2 h. The hydrated Matrigel-coated inserts for the invasion assay and the non-coated inserts for the migration assay were placed into 24-well plates containing 750  $\mu$ L of RPMI-1640 medium with 10% FBS. HuCCT1 cells (wt or *ITGB6*-ko) ( $5 \times 10^5$  cells) in serum-free medium were seeded into the insert. After incubation for 24 h at 37 °C, the cells were fixed and stained with Diff-Quik solution (Sysmex, Hyogo, Japan). The membranes were then removed and mounted on a slide. The numbers of migrated and invaded cells were counted in five random fields under a light microscope (10 $\times$  magnification), and the average value of the five fields was calculated.

#### 4.8. Wound-Healing Assay

HuCCT1 cells (wt or *ITGB6*-ko) ( $5 \times 10^4$  cells) were plated into 24-well plates and incubated for 72 h to reach confluence. After replacing the media with serum-free media, the cell monolayer was scratched with a sterile pipette tip and photographed under a light microscope at 0, 24, 48, 72, 96, and 120 h. The area of the wound was measured, and the migration rate was calculated based on the width of the 0-h timepoint (BZ-X700 Analyzer, Keyence).

#### 4.9. Colony Formation Assay

HuCCT1 cells (wt or *ITGB6*-ko) ( $5 \times 10^2$  cells) were seeded into 6-well plates and cultured (37 °C, 5% CO<sub>2</sub>) for 10 days. The cell colonies were fixed with methanol for 30 min and then stained with 0.1% crystal violet for 30 min. Five random fields were photographed under a light microscope (10× magnification), and the area of the colonies was measured using an image analyzer (BZ-X700 Analyzer, Keyence).

#### 4.10. Cell Cycle Analysis

Cells ( $1 \times 10^5$ – $10^6$ ) were trypsinized and fixed with 70% ethanol at 4 °C for at least 30 min. After washing with PBS, 50 µL of 100 µg/mL of RNase solution was added, followed by incubation at 37 °C for 20 min. Next, 25 µg/mL of propidium iodide solution was added, followed by incubation in the dark at 4 °C for 30 min, and then the cell cycle distribution was assessed in triplicate by flow cytometry (CytoFLEX, BECKMAN COULTER).

#### 4.11. RNA-Seq Analysis

RNA-seq was performed on *ITGB6*-ko 1 with single-base insertion. Total RNA was extracted from HuCCT1-wt and *ITGB6*-ko 1 cells ( $n = 3$  each) using a RNeasy Mini Kit (Qiagen). RNA-seq was performed by Takara Bio Inc. (Shiga, Japan). Sequencing libraries were constructed using the SMART-Seq v4 Ultra Low Input RNA Kit (Clontech Laboratories, Mountain View, CA, USA) for sequencing and the Nextera XT DNA Library Prep Kit and Nextera XT Index Kit v2 SetA/B/C/D (Illumina, San Diego, CA, USA) for libraries. The libraries were sequenced on a NovaSeq 6000 system (Illumina) and mapped to the human genome GRCh38 using the DRAGEN Bio-IT Platform (Illumina). Differentially expressed genes were identified using a *t*-test ( $p < 0.05$ ) and log fold change ( $\log_2 < -1$  or  $> 1$ ). To interpret the biological functions of the differentially expressed genes, gene ontology and pathway analysis were performed using DAVID v6.8 (National Institute of Allergy and Infectious Diseases) and the KEGG database. We then narrowed down the target genes using the adjusted *p*-value and log fold change ( $\log_2 < -1$  or  $> 1$ ) after the application of the Benjamini–Hochberg procedure to decrease the number of false positives.

#### 4.12. Real-Time PCR

Total RNA was extracted from HuCCT1-wt, *ITGB6*-ko 1, and *ITGB6*-ko 2 cells using an RNeasy Mini Kit (Qiagen) in accordance with the manufacturer's protocol. One microgram of total RNA was reverse-transcribed to cDNA using a QuantiTect RT Kit (Qiagen) with oligo(dT) and random hexamers in accordance with the manufacturer's instructions. Quantitative PCR was performed using Power SYBR Green Master Mix (Thermo Fisher Scientific, Waltham, MA, USA) and custom-made primers. The PCR primers used in this study were synthesized by FASMAC (Supplementary Table S4). Expression was normalized to that of glyceraldehyde-3-phosphate dehydrogenase. All reactions were performed in triplicate using the ABI 7900HT real-time PCR system (Applied Biosystems, Foster City, CA, USA).

#### 4.13. Immunohistochemistry and Evaluation

Paraffin-embedded tissue sections that were 4-µm in thickness were deparaffinized with xylene and rehydrated with graded ethanol. Antigen retrieval was performed with pH6 citrate buffer for PODXL2, and Proteinase K for integrin β6. Endogenous peroxidase was quenched with 3% H<sub>2</sub>O<sub>2</sub> in distilled water for 5 min. The slides were incubated with rabbit anti-PODXL2 antibody (1:300; Atlas Antibodies) and mouse monoclonal anti-integrin β6 (1:400; Merck) for 30 min at room temperature, followed by incubation with the secondary antibody and detection using a Histofine Simple Stain MAX PO (MULTI) (Nichirei Biosciences, Tokyo, Japan) in accordance with the manufacturer's protocol, and counterstained with hematoxylin. PODXL2 and integrin β6 expressions were considered positive when more than 5% of the tumor cells or areas showed positive staining regardless of the intensity.

#### 4.14. Statistical Analysis

Each experiment was carried out in triplicate, and the data were expressed as the mean  $\pm$  standard deviation. The data of the Transwell assays, colony formation assays, and wound-healing assays were assessed using analysis of variance (Tukey), and mRNA levels were assessed using one-way analysis of variance (Dunnett). The correlations between the clinicopathological findings and PODXL2 or integrin  $\beta 6$  expression in iCCA were assessed using Fisher's exact or  $\chi^2$  and Student's *t*-tests. The correlation between PODXL2 expression and integrin  $\beta 6$  expression in iCCA was analyzed based on Spearman's rank correlation coefficient. A  $p < 0.05$  was considered significant.

**Supplementary Materials:** The following are available online at <https://www.mdpi.com/article/10.3390/ijms22126303/s1>.

**Author Contributions:** Conceptualization, Y.S. and T.F.; methodology, formal analysis, and investigation, M.T. and Y.S.; validation, N.M. and Y.S.; data curation, N.M.; writing—original draft preparation, Y.S.; writing—review and editing, T.F.; supervision, and project administration, M.S.; funding acquisition, Y.S. All authors have read and agreed to the published version of the manuscript.

**Funding:** This research was funded by Japan Society for the Promotion of Science (JSPS)/KAKENHI, grant number JP19K16550 and the Miyakawa Memorial Research Foundation.

**Institutional Review Board Statement:** The study was conducted according to the guidelines of the Declaration of Helsinki, and approved by the Ethics Committee of Tokyo Medical and Dental University (No. M2000-2081; 8 May 2015).

**Data Availability Statement:** The data presented in this study are available in this article or supplementary material.

**Acknowledgments:** We would like to thank Shumpei Ishikawa and Daisuke Komura, the University of Tokyo, for their helpful discussions. We also thank Masanobu Kitagawa and Kouhei Yamamoto, Tokyo Medical and Dental University, for kind gift of reagents.

**Conflicts of Interest:** The authors declare no conflict of interest. The sponsors had no role in the design, execution, interpretation, or writing of the study.

## References

- Rizvi, S.; Khan, S.A.; Hallemeier, C.L.; Kelley, R.K.; Gores, G.J. Cholangiocarcinoma — evolving concepts and therapeutic strategies. *Nat. Rev. Clin. Oncol.* **2018**, *15*, 95–111. [[CrossRef](#)] [[PubMed](#)]
- Clements, O.; Eliahoo, J.; Kim, J.U.; Taylor-Robinson, S.D.; Khan, S.A. Risk factors for intrahepatic and extrahepatic cholangiocarcinoma: A systematic review and meta-analysis. *J. Hepatol.* **2020**, *72*, 95–103. [[CrossRef](#)] [[PubMed](#)]
- Sirica, A.E.; Gores, G.J.; Groopman, J.D.; Selaru, F.M.; Strazzabosco, M.; Wang, X.W.; Zhu, A.X. Intrahepatic Cholangiocarcinoma: Continuing Challenges and Translational Advances. *Hepatology* **2019**, *69*, 1803–1815. [[CrossRef](#)] [[PubMed](#)]
- Nakanuma, Y.; Klimstra, D.; Komuta, M.; Zen, Y. Intrahepatic cholangiocarcinoma. In *WHO Classification of Tumors: Digestive System Tumours*, 5th ed.; Lokuhetty, D., White, V.A., Watanabe, R., Cree, I.A., Eds.; International Agency for Research on Cancer (IARC): Lyon, France, 2019; pp. 254–259.
- Sia, D.; Hoshida, Y.; Villanueva, A.; Roayaie, S.; Ferrer-Fabrega, J.; Tabak, B.; Peix, J.; Sole, M.; Tovar, V.; Alsinet, C.; et al. Integrative Molecular Analysis of Intrahepatic Cholangiocarcinoma Reveals 2 Classes That Have Different Outcomes. *Gastroenterology* **2013**, *144*, 829–840. [[CrossRef](#)]
- Rizvi, S.; Gores, G.J. Emerging molecular therapeutic targets for cholangiocarcinoma. *J. Hepatol.* **2017**, *67*, 632–644. [[CrossRef](#)]
- Soejima, Y.; Inoue, M.; Takahashi, Y.; Uozaki, H.; Sawabe, M.; Fukusato, T. Integrins  $\alpha v\beta 6$ ,  $\alpha 6\beta 4$  and  $\alpha 3\beta 1$  are down-regulated in cholangiolocellular carcinoma but not cholangiocarcinoma. *Hepatol. Res.* **2014**, *44*, E320–E334. [[CrossRef](#)]
- Hynes, R.O. Integrins: Bidirectional, Allosteric Signaling Machines. *Cell* **2002**, *110*, 673–687. [[CrossRef](#)]
- Kechagia, J.Z.; Ivaska, J.; Roca-Cusachs, P. Integrins as biomechanical sensors of the microenvironment. *Nat. Rev. Mol. Cell Biol.* **2019**, *20*, 457–473. [[CrossRef](#)]
- Hamidi, H.; Ivaska, J. Every step of the way: Integrins in cancer progression and metastasis. *Nat. Rev. Cancer* **2018**, *18*, 533–548. [[CrossRef](#)]
- Cooper, J.; Giancotti, F.G. Integrin Signaling in Cancer: Mechanotransduction, Stemness, Epithelial Plasticity, and Therapeutic Resistance. *Cancer Cell* **2019**, *35*, 347–367. [[CrossRef](#)]
- Koivisto, L.; Bi, J.; Häkkinen, L.; Larjava, H. Integrin  $\alpha v\beta 6$ : Structure, function and role in health and disease. *Int. J. Biochem. Cell Biol.* **2018**, *99*, 186–196. [[CrossRef](#)]

13. Desnoyers, A.; González, C.; Pérez-Segura, P.; Pandiella, A.; Amir, E.; Ocaña, A. Integrin  $\alpha v \beta 6$  Protein Expression and Prognosis in Solid Tumors: A Meta-Analysis. *Mol. Diagn. Ther.* **2020**, *24*, 143–151. [[CrossRef](#)]
14. Nieberler, M.; Reuning, U.; Reichart, F.; Notni, J.; Wester, H.-J.; Schwaiger, M.; Weinmüller, M.; Räder, A.; Steiger, K.; Kessler, H. Exploring the Role of RGD-Recognizing Integrins in Cancer. *Cancers* **2017**, *9*, 116. [[CrossRef](#)]
15. Yang, G.-Y. Integrin  $\alpha v \beta 6$  sustains and promotes tumor invasive growth in colon cancer progression. *World J. Gastroenterol.* **2015**, *21*, 7457–7467. [[CrossRef](#)]
16. Reader, C.S.; Vallath, S.; Steele, C.W.; Haider, S.; Brentnall, A.; Desai, A.; Moore, K.M.; Jamieson, N.B.; Chang, D.; Bailey, P.; et al. The integrin  $\alpha v \beta 6$  drives pancreatic cancer through diverse mechanisms and represents an effective target for therapy. *J. Pathol.* **2019**, *249*, 332–342. [[CrossRef](#)]
17. Ding, Y.-B.; Deng, B.; Huang, Y.-S.; Xiao, W.-M.; Wu, J.; Zhang, Y.-Q.; Wang, Y.-Z.; Wu, D.-C.; Lu, G.-T.; Wu, K.-Y. A High Level of Integrin  $\alpha 6$  Expression in Human Intrahepatic Cholangiocarcinoma Cells Is Associated with a Migratory and Invasive Phenotype. *Dig. Dis. Sci.* **2013**, *58*, 1627–1635. [[CrossRef](#)]
18. Li, Z.; Biswas, S.; Liang, B.; Zou, X.; Shan, L.; Li, Y.; Fang, R.; Niu, J. Integrin  $\beta 6$  serves as an immunohistochemical marker for lymph node metastasis and promotes cell invasiveness in cholangiocarcinoma. *Sci. Rep.* **2016**, *6*, 30081. [[CrossRef](#)]
19. Sun, Q.; Dong, X.; Shang, Y.; Sun, F.; Niu, J.; Li, F. Integrin  $\alpha v \beta 6$  predicts poor prognosis and promotes resistance to cisplatin in hilar cholangiocarcinoma. *Pathol. Res. Pract.* **2020**, *216*, 153022. [[CrossRef](#)]
20. Soejima, Y.; Takeuchi, M.; Akashi, T.; Sawabe, M.; Fukusato, T.  $\beta 4$  and  $\beta 6$  Integrin Expression Is Associated with the Subclassification and Clinicopathological Features of Intrahepatic Cholangiocarcinoma. *Int. J. Mol. Sci.* **2018**, *19*, 1004. [[CrossRef](#)]
21. Liao, J.-Y.; Tsai, J.-H.; Yuan, R.-H.; Chang, C.-N.; Lee, H.-J.; Jeng, Y.-M. Morphological subclassification of intrahepatic cholangiocarcinoma: Etiological, clinicopathological, and molecular features. *Mod. Pathol.* **2014**, *27*, 1163–1173. [[CrossRef](#)]
22. Hayashi, A.; Misumi, K.; Shibahara, J.; Arita, J.; Sakamoto, Y.; Hasegawa, K.; Kokudo, N.; Fukayama, M. Distinct Clinicopathologic and Genetic Features of 2 Histologic Subtypes of Intrahepatic Cholangiocarcinoma. *Am. J. Surg. Pathol.* **2016**, *40*, 1021–1030. [[CrossRef](#)]
23. Sasseti, C.; Van Zante, A.; Rosen, S.D. Identification of Endoglycan, a Member of the CD34/Podocalyxin Family of Sialomucins. *J. Biol. Chem.* **2000**, *275*, 9001–9010. [[CrossRef](#)]
24. Fieger, C.B.; Sasseti, C.M.; Rosen, S.D. Endoglycan, a Member of the CD34 Family, Functions as an L-selectin Ligand through Modification with Tyrosine Sulfation and Sialyl Lewis x. *J. Biol. Chem.* **2003**, *278*, 27390–27398. [[CrossRef](#)]
25. Kerr, S.C.; Fieger, C.B.; Snapp, K.R.; Rosen, S.D. Endoglycan, a Member of the CD34 Family of Sialomucins, Is a Ligand for the Vascular Selectins. *J. Immunol.* **2008**, *181*, 1480–1490. [[CrossRef](#)]
26. Taniuchi, K.; Furihata, M.; Naganuma, S.; Sakaguchi, M.; Saibara, T. Overexpression of PODXL/ITGB1 and BCL7B/ITGB1 accurately predicts unfavorable prognosis compared to the TNM staging system in postoperative pancreatic cancer patients. *PLoS ONE* **2019**, *14*, e0217920. [[CrossRef](#)]
27. He, S.; Du, W.; Li, M.; Yan, M.; Zheng, F. PODXL might be a new prognostic biomarker in various cancers: A meta-analysis and sequential verification with TCGA datasets. *BMC Cancer* **2020**, *20*, 1–13. [[CrossRef](#)]
28. Lin, Y.-Y.; Wang, C.-Y.; Phan, N.N.; Chiao, C.-C.; Li, C.-Y.; Sun, Z.; Hung, J.-H.; Chen, Y.-L.; Yen, M.-C.; Weng, T.-Y.; et al. PODXL2 maintains cellular stemness and promotes breast cancer development through the Rac1/Akt pathway. *Int. J. Med. Sci.* **2020**, *17*, 1639–1651. [[CrossRef](#)]
29. Liu, B.; Saber, A.; Haisma, H.J. CRISPR/Cas9: A powerful tool for identification of new targets for cancer treatment. *Drug Discov. Today* **2019**, *24*, 955–970. [[CrossRef](#)]
30. Zhan, T.; Rindtorff, N.; Betge, J.; Ebert, M.P.; Boutros, M. CRISPR/Cas9 for cancer research and therapy. *Semin. Cancer Biol.* **2019**, *55*, 106–119. [[CrossRef](#)]
31. Ran, F.A.; Hsu, P.D.; Lin, C.-Y.; Gootenberg, J.; Konermann, S.; Trevino, A.E.; Scott, D.A.; Inoue, A.; Matoba, S.; Zhang, Y.; et al. Double Nicking by RNA-Guided CRISPR Cas9 for Enhanced Genome Editing Specificity. *Cell* **2013**, *154*, 1380–1389. [[CrossRef](#)] [[PubMed](#)]
32. Eberlein, C.; Kendrew, J.; McDavid, K.; Alfred, A.; Kang, J.S.; Jacobs, V.N.; Ross, S.J.; Rooney, C.; Smith, N.R.; Rinkenberger, J.; et al. A human monoclonal antibody 264RAD targeting  $\alpha v \beta 6$  integrin reduces tumour growth and metastasis, and modulates key biomarkers in vivo. *Oncogene* **2012**, *32*, 4406–4416. [[CrossRef](#)] [[PubMed](#)]
33. Hausner, S.H.; Bold, R.J.; Cheuy, L.Y.; Chew, H.K.; Daly, M.E.; Davis, R.A.; Foster, C.C.; Kim, E.J.; Sutcliffe, J.L. Preclinical Development and First-in-Human Imaging of the Integrin  $\alpha v \beta 6$  with [18F] $\alpha v \beta 6$ -Binding Peptide in Metastatic Carcinoma. *Clin. Cancer Res.* **2018**, *25*, 1206–1215. [[CrossRef](#)] [[PubMed](#)]
34. Miyagiwa, M.; Ichida, T.; Tokiwa, T.; Sato, J.; Sasaki, H. A new human cholangiocellular carcinoma cell line (HuCC-T1) producing carbohydrate antigen 19/9 in serum-free medium. *Vitr. Cell. Dev. Biol. - Anim.* **1989**, *25*, 503–510. [[CrossRef](#)] [[PubMed](#)]
35. Kusaka, Y.; Tokiwa, T.; Sato, J. Establishment and characterization of a cell line from a human cholangiocellular carcinoma. *Res. Exp. Med.* **1988**, *188*, 367–375. [[CrossRef](#)] [[PubMed](#)]